Magn Reson Mater Phy (2016) 29:811–822
DOI 10.1007/s10334-016-0566-z

RESEARCH ARTICLE

# Denoising of MR spectroscopic imaging data using statistical selection of principal components

**Abas Abdoli[1] · Radka Stoyanova[2] · Andrew A. Maudsley[1]**

Received: 13 January 2016 / Revised: 9 May 2016 / Accepted: 11 May 2016 / Published online: 3 June 2016


**Abstract**
*Objectives* To evaluate a new denoising method for MR spectroscopic imaging (MRSI) data based on selection of signal-related principal components (SSPCs) from principal components analysis (PCA).
*Materials and methods* A PCA-based method was implemented for selection of signal-related PCs and denoising achieved by reconstructing the original data set utilizing only these PCs. Performance was evaluated using simulated MRSI data and two volumetric in vivo MRSIs of human brain, from a normal subject and a patient with a brain tumor, using variable signal-to-noise ratios (SNRs), metabolite peak areas, Cramer-Rao bounds (CRBs) of fitted metabolite peak areas and metabolite linewidth.
*Results* In simulated data, SSPC determined the correct number of signal-related PCs. For in vivo studies, the SSPC denoising resulted in improved SNRs and reduced metabolite quantification uncertainty compared to the original data and two other methods for denoising. The method also performed very well in preserving the spectral linewidth and peak areas. However, this method performs better for regions that have larger numbers of similar spectra.
*Conclusion* The proposed SSPC denoising improved the SNR and metabolite quantification uncertainty in MRSI, with minimal compromise of the spectral information, and can result in increased accuracy.

✉ Andrew A. Maudsley
amaudsley@miami.edu

[1] Department of Radiology, University of Miami School of Medicine, 1150 NW 14th St, Suite 713, Miami, FL 33136, USA

[2] Department Radiation Oncology, University of Miami School of Medicine, Miami, FL, USA

**Keywords** MRSI denoising · PCA denoising · SVD denoising · Low-rank denoising · Spectral analysis

## Introduction

MR spectroscopic imaging (MRSI) enables mapping distributions of several tissue metabolites that are of interest for noninvasive clinical diagnostic purposes, particularly for studies in the brain [1]. The technical challenges in acquiring data from low-concentration metabolites require a compromise in the spatial resolution and signal-to-noise ratio (SNR) of the measurement, which can decrease the value for clinical applications. While increased SNRs can be achieved by signal averaging, this is frequently impractical for clinical studies because of the increased scan times and susceptibility to movement artifacts.

An alternative approach to improving the SNR, and thereby reducing the uncertainty of the MRSI analysis, is to reduce noise in the data as part of the reconstruction procedure. A simple approach is to smooth the data in both the spatial and spectral domains using, for example, a Gaussian function [2], which also results in decreased spatial resolution or increased spectral linewidth, respectively [3]. Another popular approach is the thresholding of the data in a transformed domain, such as wavelet and time-frequency, followed by inverse transformation. Ancino-De-Geiff et al. [4] proposed the use of wavelet shrinkage for denoising of MRS data. In this method, the data are transformed to a decorrelated domain by an orthonormal series generated by wavelets, and then the denoising is applied through thresholding of wavelet coefficients and inverse transformation [5]. Later, Ojanen et al. [6] proposed the minimal description length method to find the optimal number of wavelet coefficients for the denoising of electrophoresis and mass

spectroscopy signals. Laruelo et al. [7] proposed a new wavelet-based denoising technique, which accounts for signal regularity across the spectral and spatial domains without altering the spectral resolution. Their method includes a proximal algorithm for a fast convex optimization to find the optimal number of wavelet coefficients. They reported improvements in retaining the spectral lineshapes compared to the convolution smoothing by a Hanning function [7]. Ahmed [8] proposed consecutive projections of the noisy MRS data in different domains in conjunction with noise filtration for each domain. For these projections, a set of stable, linear time-frequency transforms was applied with different resolutions [9], and improvements over the wavelet shrinkage method for $^{31}$P single voxel data were reported [8]. However, for consideration of this method for volumetric MRSI data, which can be on the order of $10^5$ spectra, the computational cost of using multiple projections must also be considered.

In a different approach, the denoising can be applied prior to or during MRS signal reconstruction using explicit parametric modeling approaches [10, 11]. Eslami and Jacob [10] proposed a reconstruction scheme for MRSI data that results in a sparser representation of the spectral data, which enables the separation and suppression of the noise as well as lineshape distortions. Nguyen et al. [11] applied a similar approach with the addition of spectral prior knowledge estimated from k-space data.

It is often assumed that the signal-related (noiseless) data are a lower rank subspace of the original data. Low-rank modeling with recent advances in its algorithm has become a popular method in the medical imaging field [12–14]. Singular value decomposition (SVD) and principal component analysis (PCA) provide a representation of complex data in a lower dimensional space that is defined by the significant PCs (principal component directions) [15, 16]. MRSI data can be represented as a product of: (1) the PCs, which are orthonormal and ordered by the decreasing amount of commonality in the data they represent; (2) their scores or magnitudes, which are the projections of the data onto the corresponding PC. The total number of PCs is usually much larger than the number of independent variations in the data set. For instance, in vivo MRSI data with 1024 points in the frequency domain will result in 1024 PCs, but if we assume that there are 10 observed metabolite spectral patterns the amplitude, frequency, phase and linewidth variations will result in ~40 signal-related PCs [17, 18], and the remaining PCs will be noise-related. Reconstructing the data using only the significant PCs while ignoring the higher noise-related ones will effectively reduce the noise in the data.

For denoising of MRSI data, Zhu et al. [19] proposed a PCA denoising technique based on a deformable shape-intensity model. They reported increased SNR up to 2.1 times without distorting spectral lineshapes and linewidths. Nguyen et al. [20] proposed a low-rank approximation (LORA) scheme that exploits two low-rank structures. The first structure is derived on the assumption that spatial and temporal variations in MRS data are separable, and the second one is calculated based on the linear predictability assumption in temporal dimension. This study reported a better performance of LORA denoising compared to the wavelet shrinkage and Gaussian smoothing in terms of SNR and spectral quality [20]. Kasten et al. [21] proposed a data-driven, low-rank component analysis for MRSI in which a generative model is estimated from the raw data via a regularized variation framework that minimizes the approximation error within the subspace.

One of the challenges of low-rank denoising is the selection of the optimal rank for approximation of the noise-free signal. In the report of Nguyen et al. [20] it was assumed that the rank of the noiseless data is equal to $N$, if the $N$th and $(N + 1)$th eigenvalues of the original data are greater (or equal) and less (or equal) than the Euclidean norm of the estimated noise, respectively. They also applied the Akaike information criterion [22] where the noiseless data are assumed to be a low-rank Hankel matrix and the noise to be a Gaussian Hankel matrix [20].

Volumetric whole-brain MRSI data sets present an additional challenge for the denoising techniques in that they can contain a wide range of data quality and include regions prone to increased artifacts due to contamination from residual water and unsuppressed subcutaneous lipid signals. Therefore, it is very likely that the spectral decomposition of the data includes PCs that only represent 'unwanted' signal artifacts. Thus, it is necessary to examine the information carried by each PC to filter out those that are dominated by either artifact or noise.

In this study a spatial-spectral low-rank method was developed for denoising of volumetric $^1$H MRSI data of the brain that was combined with a new approach for selection of the significant signal-related PCs obtained from PCA. In this method, PCs are selected using a statistical test that examines the relative information content describing the metabolite signal. To improve the performance, the denoising step is applied after correction for B0 and phase shifts, which results in a smaller number of signal-related PCs relative to the uncorrected data.

## Materials and methods

### Theory

Let $s_i(\omega)$ be the noise-free spectrum of voxel $i$, for $i = 1, \ldots, N$ where $N$ is the total number of voxels and $\omega$ is the frequency. Assuming $s_i(\omega)$ contains $M$ spectral peaks

and $\boldsymbol{f}_j(\omega)$, $j = 1, \ldots, M$, represents the normalized spectral shape of the $j$th peak, $\boldsymbol{s}_i(\omega)$ can be represented as the weighted sum of the shapes:

$$\boldsymbol{s}_i(\omega) = \sum_{j=1}^{M} \boldsymbol{A}_j \boldsymbol{f}_j(\omega) \tag{1}$$

where $\boldsymbol{A}_j$ is the amplitude of $jth$ spectral peak in voxel $i$. Let $\bar{\boldsymbol{s}}_i(\omega)$ be the acquired MRS spectrum:

$$\bar{\boldsymbol{s}}_i(\omega) = \boldsymbol{s}_i(\omega) + \epsilon \tag{2}$$

where $\epsilon$ is complex Gaussian noise with mean 0 and standard deviation $\sigma$, i.e., $\epsilon \in N(0, \sigma^2)$. For volumetric MRSI, let us reform the data to a two-dimensional complex matrix $\bar{\boldsymbol{S}}(r, \omega)$ with $r$ and $\omega$ being the spatial and frequency domains, respectively. Therefore, each row will represent a spectrum, $\bar{\boldsymbol{s}}_i(\omega)$, and the total number of rows ($r$) would be $N$. Let $\boldsymbol{S}(r, \omega)$ be the corresponding 'noiseless' complex matrix with $\boldsymbol{s}_i(\omega)$ in its rows. Therefore, for the volumetric MRSI, Eq. 2 can be represented as:

$$\bar{\boldsymbol{S}}(r, \omega) = \boldsymbol{S}(r, \omega) + \epsilon \tag{3}$$

PCA is a standard statistical technique for decomposition of $\bar{\boldsymbol{S}}(r, \omega)$ along the axes of the PCs, which are ordered by the decreasing amount of commonality in the data they represent:

$$\bar{\boldsymbol{S}}(r, \omega) = \boldsymbol{Z}(r, \omega) \cdot \boldsymbol{P}(\omega, \omega) \tag{4}$$

where $\boldsymbol{Z}(r, \omega)$ is the matrix of PC scores, and $\boldsymbol{P}(\omega, \omega)$ is the PCs matrix. In the case that the amplitudes of the metabolite peaks $\boldsymbol{A}_j$ (Eq. 1) vary independently from each other, PCA will yield $L$ significant PCs. The rest of the PCs will be noise related. The spectral matrix can be reconstructed only with the first $L$ PCs and thus the data will be 'denoised,' i.e.:

$$\bar{\boldsymbol{S}}(r, \omega)_L \approx \boldsymbol{S}(r, \omega)_L \tag{5}$$

where subscript $L$ indicates the low rank of the matrix based on $L$ significant signal-related PCs. Determining the rank $L$ in in vivo MRSI data, however, is quite challenging as it is not known a priori how many spectral patterns are in the data, and, more importantly, there are added noise and additional features from variations in frequency, phase, lineshape and baseline, which exacerbate the problem.

## Method

The proposed method, statistical selection of principal components (SSPC), determines the signal related PCs in $\bar{\boldsymbol{S}}(r, \omega)$. The technique is based on examining each PC and comparing the variance in frequency regions with known metabolites with the variance in the 'noise' regions. For this purpose, Levene's test [23] was performed to assess the equality of variances between these two regions. Similar to the F-test, Levene's test is a variance equality test that can handle the non-normality of data. While in Eq. 2 the noise is assumed Gaussian, it should be noted that any apodization, zero-filling or spatial filtering introduces correlation, and the noise in MRS after these standard pre-processing procedures cannot be considered normally distributed. Also, the peak amplitudes within the metabolite region generally are not normally distributed. After performing Levene's test, a threshold was applied to the significant difference ($p$ value) calculated by the test to retain the significant PCs and construct the $\bar{\boldsymbol{S}}(r, \omega)$. The selection is applied to all PCs and the result need not be consecutive, i.e., $\mathrm{PC}_{i+1}$ may be included while $\mathrm{PC}_\mathrm{i}$ is excluded. In this method, the total number of selected PCs would be equal to the rank $L$ of $\bar{\boldsymbol{S}}(r, \omega)$. The choice of the $p$ value threshold depends on the noise level in the data set and will be determined by the user. An estimate for the threshold value can be obtained by performing Levene's test for two noise-only regions in the last PCs that are noise-related PCs; however, the threshold value can be increased to retain more PCs.

### Simulated MRSI data

Simulated volumetric MRSI data sets were generated for Cartesian k-space sampling using a function in the MIDAS (metabolite image data analysis system) software package [24]. To examine the performance of the PC selection, a MRSI data set was created for a simple abstract object consisting of three overlapping spherical volumes, each characterized by a different spectral pattern, labeled line 1, line 2 and line 3 (Fig. 1a). Spectroscopy signals were generated with Gaussian lineshapes and constant amplitudes over each region with relative values of 0.8, 0.7 and 1.0. Gaussian noise with mean value 0 and standard deviation of 0.08 was added in the time domain. The spatial resolution of the simulated data sets was $64 \times 64$ voxels in-plane and 4 voxels through-plane. To examine the effect of frequency and phase shifts, a second data set was generated with randomly shifted phase and frequency between $-30°$ and $+30°$, and $-6$ Hz to 6 Hz, respectively.

A third data set was generated to resemble the volumes and metabolites in an in vivo brain MRSI that included a small lesion with a different spectral pattern. The primary volume had an ellipsoidal shape containing subregions with different spectral patterns that represented a lipid ring, normal brain tissue, ventricles containing only a water signal and a small region representing a brain lesion (blue region in Fig. 3). In addition, spatial variations of all simulated spectral peaks were created throughout the whole object following a synchronous cubic distribution pattern for all metabolites. The metabolite region included simulated

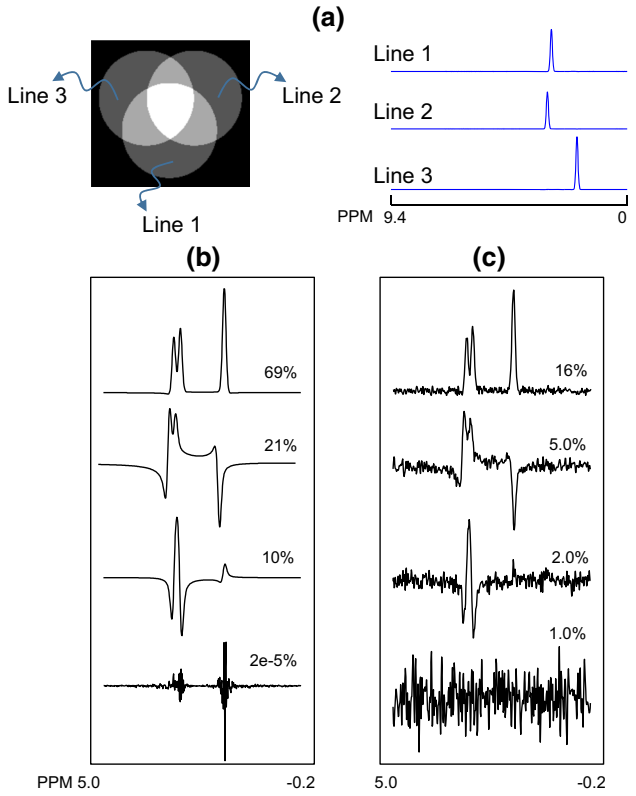


**Fig. 1** MRS data were simulated by generating an abstract object, shown in **a**, consisting of three overlapping spherical volumes. Each volume contained a single peak line, shown on the *right* as line 1, line 2 and line 3. The real part of the first four PCs with their corresponding normalized eigenvalues, obtained from PCA analysis of the simulated data set **b** before and **c** after adding Gaussian noise

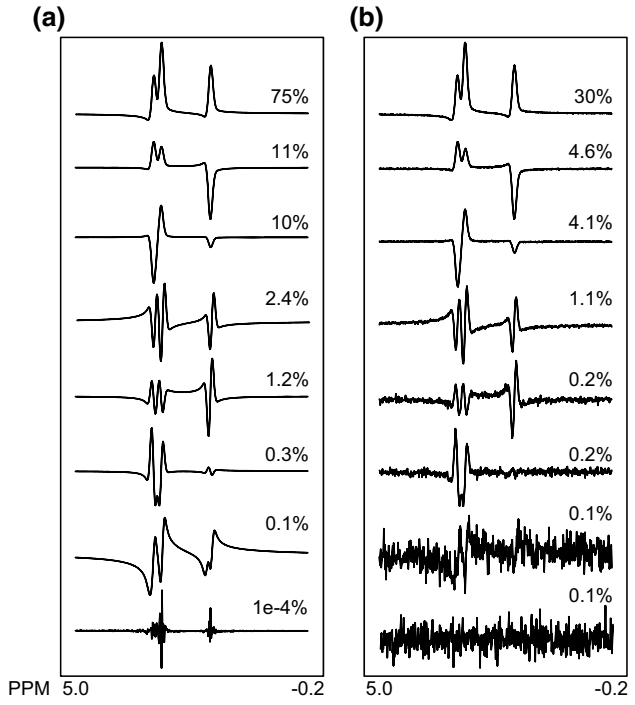


**Fig. 2** Phase and frequency shifted MRS data were simulated by generating an abstract object consisting of three overlapping spherical volumes. The real part of the first eight PCs with their corresponding normalized eigenvalues, obtained from PCA analysis of the simulated data set **a** before, and **b** after, adding Gaussian noise

resonances for N-acetylaspartate ($NAA_{sim}$), total creatine ($Cr_{sim}$) and total choline ($Cho_{sim}$), whereas in the lesion the NAA peak was set to zero, and an overlapped doublet for lactate ($Lac_{sim}$) was included.

### In vivo MRSI data

Volumetric MRSI data of one normal subject (male, 31 years old) and one brain tumor subject (female, 49 years old) were obtained at 3 T (Siemens Trio) with eight-channel detection. Subjects were scanned after obtaining signed informed consent in accordance with the procedure approved by our Institutional Review Board. These data were acquired using a spin-echo acquisition with two-dimensional phase encoding, echo-planar readout in the $k_y$-time dimensions, frequency-selective water suppression and TR/TE = 1551/17.6 ms. Sequence details have been provided elsewhere [25–27]. The acquisition included a water-reference data set obtained in an interleaved manner with identical spatial parameters as the metabolite MRSI. MRSI acquisition was preceded by an inversion-recovery preparation, with TI = 198 ms, to suppress the signal from subcutaneous lipids [25, 27]. A *T*1-weighted image (MPRAGE, Magnetization Prepared Rapid Gradient Echo) at 1-mm resolution (TR/TE/TI = 2300/2.4/930 ms) was also acquired for each study.

All data were processed using the MIDAS software package [24]. The processing steps included resampling of the echo-planar imaging (EPI) readout with combination of odd and even echo readouts [28], zero-filling in the spatial domain from 50 × 50 × 18 points to 64 × 64 × 32 points, zero-filling in the frequency domain from 500 points to 1024 points, Fourier transformation in all three spatial dimensions and multichannel combination [29]. Spatial smoothing (Gaussian, damping factor of 2.0) was applied as a convolution in the spatial domain after spatial-spectral Fourier transformation, B0 correction and lipid k-space extrapolation [30]. The resolution of the reconstructed metabolite images corresponded to a voxel volume of 1.55 ml calculated at full width at half maximum.

A high SNR reference data set was also created from the normal subject data set by averaging the MRSI data from 64 × 64 voxels in-plane and 32 voxels through-plane to 10 × 10 voxels in-plane and 10 voxels through-plane. The averaging was performed after application of the processing steps mentioned above. To remove noisy

and contaminated averaged spectra based on LW and CSF partial volume criteria, parametric spectral fitting [31] was performed to derive the LW from NAA, Cre and Cho resonances. A threshold of $2 < LW < 8$ was then applied to filter out the unwanted averaged spectra. A noisy version of this data set was then generated by adding a Gaussian noise with mean value 0, standard deviation 0.08, based on the maximum amplitudes of NAA in the averaged data. The purpose of this study was to examine the performance of the SSPC denoising method in improving the metabolite quantification for in vivo data sets.

To increase the effectiveness of the SSPC denoising for the in vivo data sets, the spectral phase and frequency variations were corrected prior to denoising. This was achieved using two steps. First, following spatial reconstruction a time-domain phase-correction function was applied at each voxel location, with the correction function obtained from the unsuppressed water acquisition. Because some phase variations still remained across the image, a second processing step was applied that used spectral fitting of the primary resonances, consisting of NAA, Cre and Cho singlet resonances only, and then the phase and frequency terms determined from this analysis as a correction to the data were applied. Following denoising, the parametric spectral fitting [31] was again performed to obtain maps of NAA, Cr and Cho, myo-inositol and glutamate plus glutamine (Glx).

For data that had the SSPC denoising applied, no spectral smoothing was applied during processing. For comparison to standard processing methods, data were also processed using Gaussian apodization of the time data, prior to spectral Fourier transformation, for a relatively small 2-Hz line-broadening and a value more typically used (for 3 T) of 5-Hz line-broadening.

### Data analysis

SSPC denoising performance was compared with: (1) spectral apodization using Gaussian smoothing and (2) conventional PCA denoising. For the second method, the rank $L$ was found using the SSPC scheme, and the same rank was applied for the PCA reconstruction using the first $L$ consecutive PCs. It should be mentioned that the conventional PCA procedure is equivalent to the first part of the LORA [20] denoising scheme. Since the second part of LORA denoising, which utilizes the Cadzow algorithm [32] for each spectrum, is not coupled to the first part, results of comparisons between the conventional PCA and SSPC denoising would also be valid for the first part of LORA denoising.

For the SSPC method, the noise and signal regions in the PCs are identified in the same manner as in the spectra, with the noise region being the first 150 points (9.4–7.90 ppm) and the metabolite region from 4.0 to 1.5 ppm. Qualitative comparisons between individual spectra obtained from different denoising methods are presented for each study. Metabolite peak areas and their Cramer-Rao bound (CRB), metabolite peak area ratios, linewidth (LW) and SNR were used as the measures for quantitative comparisons. SNR was calculated using the fitted NAA area over the standard deviation (SD) of the noise in the spectral domain, with the noise measurement taken from the last 100 points (0.64 to −0.35 ppm) of the spectrum. NAA peak area was used for the SNR calculation since it accounts for changes in linewidth. For the SNR calculation within the tumor region, the fitted Cho area was used instead of the fitted NAA area. In both studies, the SNR measurement was done after application of the spectral fitting. To examine the spatial distributions of the relative performance in more detail, images of the metabolite peak area, CRB, LW and SNR were generated for the study of a normal subject. The coefficient of variation (CV) of the root mean square error (RMSE) was also used to calculate errors in the NAA, Cho and Cr fitted areas for the simulated data as

$$\mathrm{CV}_{\mathrm{RMSE}} = \frac{\sqrt{\frac{\sum_{i=0}^{N}(\boldsymbol{M}_{\mathrm{ref}}-\boldsymbol{M})^2}{N}}}{\bar{\boldsymbol{M}}} \tag{6}$$

where $M_{\mathrm{ref}}$ is the known (reference) value at voxel $i$, $M$ is the fitted area at that voxel, and $\bar{\boldsymbol{M}}$ is the mean value of the reference areas over N voxels in the ROI.

## Results

### Simulated MRSI data

Figure 1 shows the central slice from the first simulated data set and the constituent spectral patterns. PCA was applied to the data before and after adding random noise. The real part of the first four PCs with their corresponding normalized eigenvalue percentages are shown in Fig. 1b, c. In the first case, the first three PCs contained 100 % of the information for reconstruction of the noiseless data. The shape of the fourth PC with only 2E −5 contribution can be considered as the numerical error of the PCA algorithm. With added noise (Fig. 1c) the first three PCs have only 23 % of the total variance; however, the PC shapes remained the same as in the noiseless data. The contribution of the fourth PC was increased to 1 % because of the presence of the noise. In both cases, SSPC determined that the first three PCs were signal-related using 0.01 as the $p$ value threshold for Levene's test. PCs for the second simulated data set are shown in Fig. 2. In this case the number of signal-related PCs was increased to seven because of the variations in the phase and frequency. The

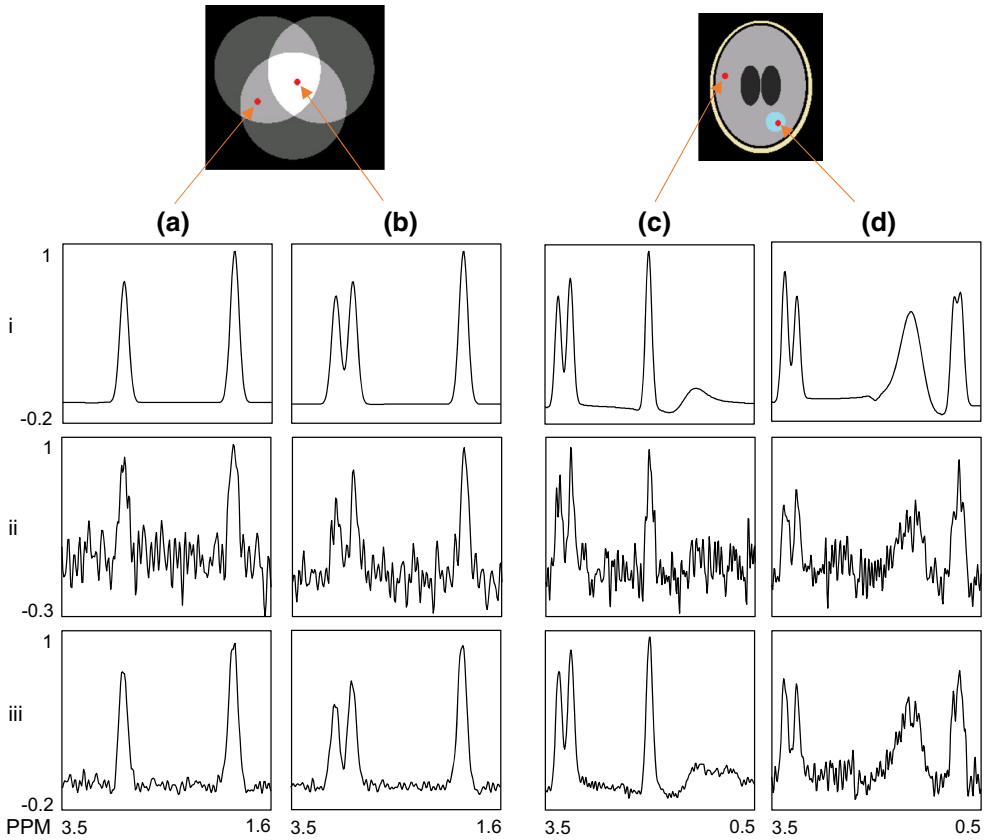


**Fig. 3** Example spectra from both simulation studies. Spectra in columns **a** and **b** show results for two voxels selected from the regions indicated in the abstract object; **c**, **d** show results for two voxels selected from the regions indicated in the ellipsoidal object. The spectra in each row are as follow: *(i)* noise-free simulated data, *(ii)* simulated after addition of random noise and *(iii)* denoised data using SSPC

SSPC method also detected seven signal-related PCs using 0.01 as the $p$ value threshold for Levene's test. This result shows that with additional variability in the data, the number of signal-related PCs is increased; however, as long as there is a significant difference between signal variations and noise variations in a given PC, the SSPC method can detect and use that PC regardless of shifts in frequency and phase. However, if the frequency and phase shifts are small, such that the difference between the shifted spectrum and corrected spectrum is less than the noise level, they can be ignored. Therefore, it is recommended to perform the SSPC denoising after the phase and frequency corrections.

Figure 3 shows example spectra from the simulation studies and the distributions used to generate the simulated MRSI data. For the simulated brain (Fig. 3c, d), this consisted of regions containing lipid signals (shown in light yellow), normal metabolites (gray), water (dark gray) and abnormal metabolite signals (blue). SSPC determined that the first four PCs were signal-related using 0.01 as the $p$ value threshold for Levene's test.

Two noise-free spectra from each of the simulated data sets are shown in the top row in Fig. 3. The spectrum in Fig. 3a (i) is selected from an area of overlap of two volumes and shows two signals, while that shown in Fig. 3b (i) is from the intersection of all three volumes and contains three signals. The examples from the simulated data set shown in Fig. 3c, d are selected to represent "normal" (relatively equal Cr and Cho peaks and high NAA) and a small region of "tumor" (increased Cho, no NAA and large lactate doublet). The second row shows the data after adding random noise, and the last row shows the results after the SSPC denoising. The results in row (iii) show that the SSPC denoising had good performance in removing the noise and preserving the peak heights, indicating no loss of information. Note that the reconstructed "tumor" spectrum, Fig. 3d (iii), is noisier than that from the "normal" region. The tumor spectra are associated with a relatively small volume, and therefore they contribute a small fraction of the total variance. As the PCs are ordered by the amount of commonality in the data they explain, the first few PCs are dominated by the signal from the 'normal' volumes. The

**Table 1** Simulated metabolite peak area ratios and SNR for the simulated MRS data

| | Voxel 1 | | | Voxel 2 | | |
|---|---|---|---|---|---|---|
| | $NAA_{sim}/Cr_{sim}$ | $NAA_{sim}/Cho_{sim}$ | SNR | $Lac_{sim}/Cr_{sim}$ | $Lac_{sim}/Cho_{sim}$ | SNR* |
| Simulated data | 1.228 | 4.147 | – | 0.362 | 0.951 | – |
| Simulated data plus Gaussian noise | 1.369 | 5.337 | 109.5 | 0.602 | 1.404 | 78.4 |
| SSPC (0.01) | 1.185 | 4.214 | 584.1 | 0.425 | 1.351 | 181.5 |

The $p$ value threshold of the SSPC denoising was 0.01

* For voxel 2, the SNR was calculated using the $Cho_{sim}$ peak area instead of $NAA_{sim}$

**Table 2** CV of RMSEs for $NAA_{sim}$, $Cr_{sim}$ and $Cho_{sim}$ fitted areas

| | ROI 1 | | | ROI 2 | |
|---|---|---|---|---|---|
| | $RMSE_{NAA}$ | $RMSE_{Cr}$ | $RMSE_{Cho}$ | $RMSE_{Cr}$ | $RMSE_{Cho}$ |
| No denoising | 0.064 | 0.075 | 0.086 | 0.334 | 0.280 |
| Gaussian apodization | 0.064 | 0.081 | 0.089 | 0.630 | 0.537 |
| SSPC | 0.043 | 0.024 | 0.029 | 0.333 | 0.266 |

ROI 1 is located outside of the tumor region, and ROI 2 is within the tumor region

tumor-related variance is in higher order PCs, which in turn contain more noise. These higher order PCs do not contribute to the reconstruction of the normal signals, hence the high SNR and conversely the lower SNR in the "tumor" spectrum.

For quantitative comparisons, the metabolite peak area ratios and SNR obtained from denoising of the simulated MRS data are presented in Table 1. After the application of SSPC denoising, the SNR for voxel 1 was increased by 433 % and for voxel 2 by 131 %. The errors for the $NAA_{sim}/Cr_{sim}$ and $NAA_{sim}/Cho_{sim}$ ratios for voxel 1 were also reduced by 69 % and 94 %, respectively. For voxel 2, the $Cho_{sim}$ peak was used instead of $NAA_{sim}$. The improvements in reducing errors for the $Lac_{sim}/Cr_{sim}$ and $Lac_{sim}/Cho_{sim}$ ratios after the application of denoising were 73 % and 12 %, respectively. Additional studies (results not shown) examined the denoising of the data using only the first three PCs and the first five PCs. The former resulted in removing the $Lac_{sim}$ peaks in the small lesion region, and the latter added more noise to the data with no improvement in peak area ratios.

Table 2 presents the coefficient of variation (CV) of the root mean square error (RMSE) of the $NAA_{sim}$, $Cr_{sim}$ and $Cho_{sim}$ areas for an ROI located outside of the tumor region (25 voxels) and for $Cr_{sim}$ and $Cho_{sim}$ within the tumor region (25 voxels). The values are compared with those obtained using Gaussian apodization of 5 Hz and the original data. These results show that the SSPC denoising reduced errors in ROI 1 by 33, 68 and 66 % for $NAA_{sim}$, $Cr_{sim}$ and $Cho_{sim}$ fitted areas, respectively, relative to the analysis of the original data. The improvements in the tumor region (ROI 2) were smaller with the maximum of 5 % reduction of error for the $Cho_{sim}$ area. The $CV_{RMSE}$ values increased for the case where Gaussian apodization was applied, which we believe is due to the increased linewidth that notably affected fitting of the closely overlapping peaks of $Cr_{sim}$ and $Cho_{sim}$.

## In vivo MRSI data

The aim of the next study was to examine the performance of the SSPC denoising applied to a MRSI data set of a normal subject. Maps of the peak areas of two metabolites ($Cr_{Area}$, $Glx_{Area}$), their corresponding CRBs, LWs and SNRs are shown in each row in Fig. 4. The use of conventional spectral apodization of 2-Hz or 5-Hz line Gaussian smoothing, shown in Fig. 4b, c, resulted in increased SNRs and reduced CRBs compared to the raw data, but also increased the metabolite LW, especially for 5-Hz line smoothing. To ensure a fair comparison between the conventional PCA and SSPC denoising methods, the same number of PCs, $L = 224$, were used for Fig. 4d, e, and 65 PCs, $L = 65$, were used for Fig. 4f, g. For these examples the number of PCs selected, $L$, was based on the value determined in the SSPC denoising approach with a $p$ value threshold of 10E−5 or 10E−10, and the first $L$ consecutive PCs were used for the conventional PCA approach. It can be observed that the SSPC denoising (Fig. 4e, g) performed better than the conventional PCA denoising (Fig. 4d, f) in terms of the CRB and SNR. The visual improvements in metabolite peak area images were more prominent for the lower concentration metabolite, $Glx_{Area}$, compared to the higher concentration metabolite, $Cr_{Area}$. By comparing Fig. 4e, g, it can be observed that decreasing the $p$ value threshold from 1E−5 to 1E−10 improved the SNRs and

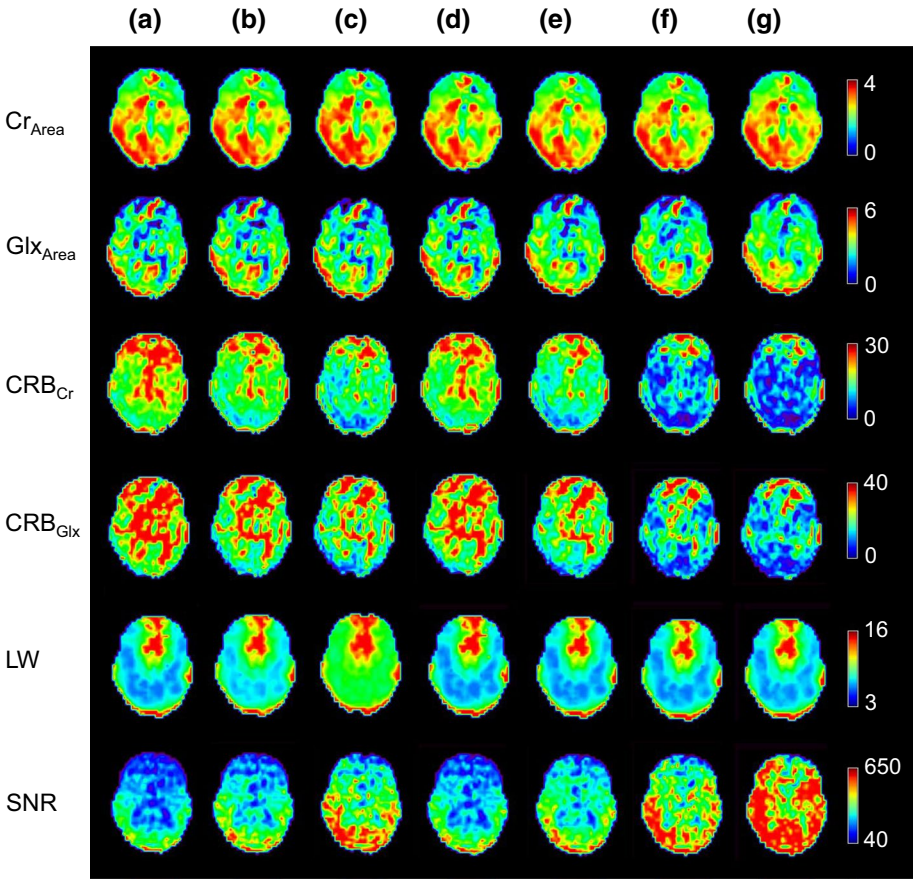


**Fig. 4** Images of denoising results for a mid-axial slice for a volumetric MRSI study of a normal subject. Results from the spectral fitting are shown in each row for different processing in each column for *a* acquired data with no spectral smoothing, *b* Gaussian apodization (2 Hz), *c* Gaussian apodization (5 Hz), *d* PCA denoising using the first 224 PCs, *e* SSPC denoising with a threshold of 1E−5 (the algorithm found 224 PCs for this threshold), *f* PCA denoising using the first 65 PCs and *g* SSPC denoising with a threshold of 1E−10 (the algorithm found 65 PCs for this threshold)

CRBs without compromising the metabolite information such as the LW and metabolite peak area.

For the second in vivo study, the high SNR averaged data were used as the reference for the evaluation of the SSPC denoising performance. The SSPC denoising was applied on the noisy data that were generated by adding Gaussian noise to the averaged data, and then its results were compared to the original averaged data. The results for analysis of NAA, which has a strong signal with a good SNR, and Glx, which exhibits a broad multiplet structure with a low SNR, are shown in Fig. 5. In Fig. 5a, the fitted NAA area results, obtained at multiple voxels before (orange) after (blue) application of the SSPC denoising, are plotted against the corresponding reference data result. It can be seen that the fitted NAA areas are clustered toward the center line with $R^2 = 0.91$ for the denoised result compared to the noisy data with $R^2 = 0.90$. As expected, the improvement is more evident for Glx (Fig. 5b), which showed a 14 % increase in $R^2$. This result illustrates that the denoising reduces uncertainty of the parametric spectral fitting.

One of the main challenges of denoising methods is to retain information in small regions of interest, such as small tumors, that have very different signal compositions compared to larger regions of the brain. Therefore, the aim of the third in vivo study was to investigate the performance of the SSPC denoising method inside and outside of a small tumor region. Figure 6 shows an MRI that identifies a tumor on the right side of the image (left side of the brain), with a gross tumor volume of 7.5 ml. Two example spectra, one from a voxel located in the normal-appearing white matter region on the opposite side of the tumor region (voxel 1) and one from a voxel within the tumor region (voxel 2), are also shown for the original data and following different denoising approaches. A visual evaluation of spectra in Fig. 6a (iii), (iv) indicates that the SSPC denoising performed better than the conventional PCA denoising. The SSPC result with the $p$ value threshold of 1E−10, Fig. 6a (v), appears less noisy compared to other methods. For voxel 2, the denoised spectra are similar in appearance; however, the spectrum shown in Fig. 6b (v) obtained from the SSPC denoising with the $p$ value threshold of 1E−10 appears less noisy and has a smaller Glx peak height compared to the other spectra.

Table 3 presents the $CRB_{Cr}$, $CRB_{Glx}$ and SNR for the two selected voxels. The SSPC denoising with 1E−10 threshold increased the SNR from 92 to 418, or 355 %. However, for voxel 2 this improvement was 169 %, which was more than two times smaller than the improvement for voxel 1. The reason for this result is that the denoising algorithm will perform

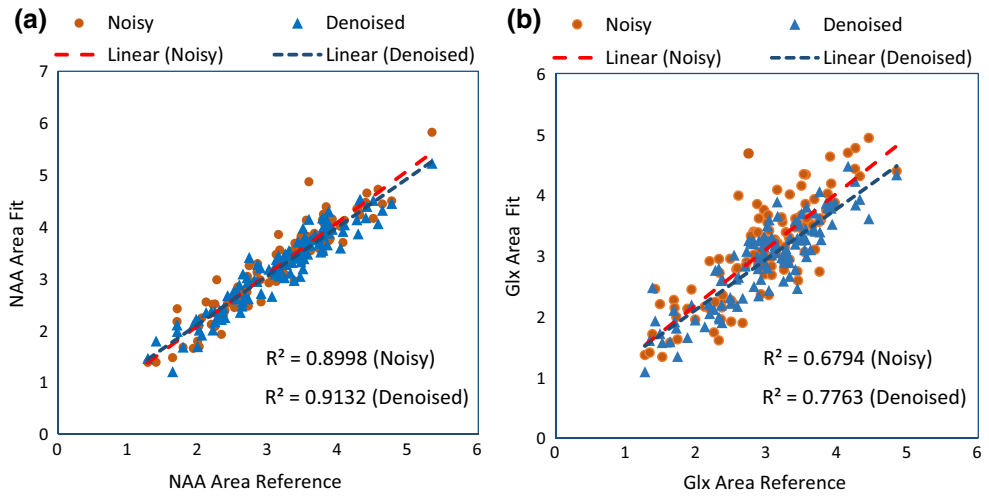


**Fig. 5** Comparison of the SSPC denoising results against a high SNR reference data set. **a** Regression *plots* for the NAA area obtained from the noisy and denoised data against the NAA area from the reference; **b** regression *plots* for Glx area obtained from the noisy and denoised data against the Glx area from the reference. The results for the noisy data and its linear regression are shown in *orange*, and those for the denoised data are shown in *blue*

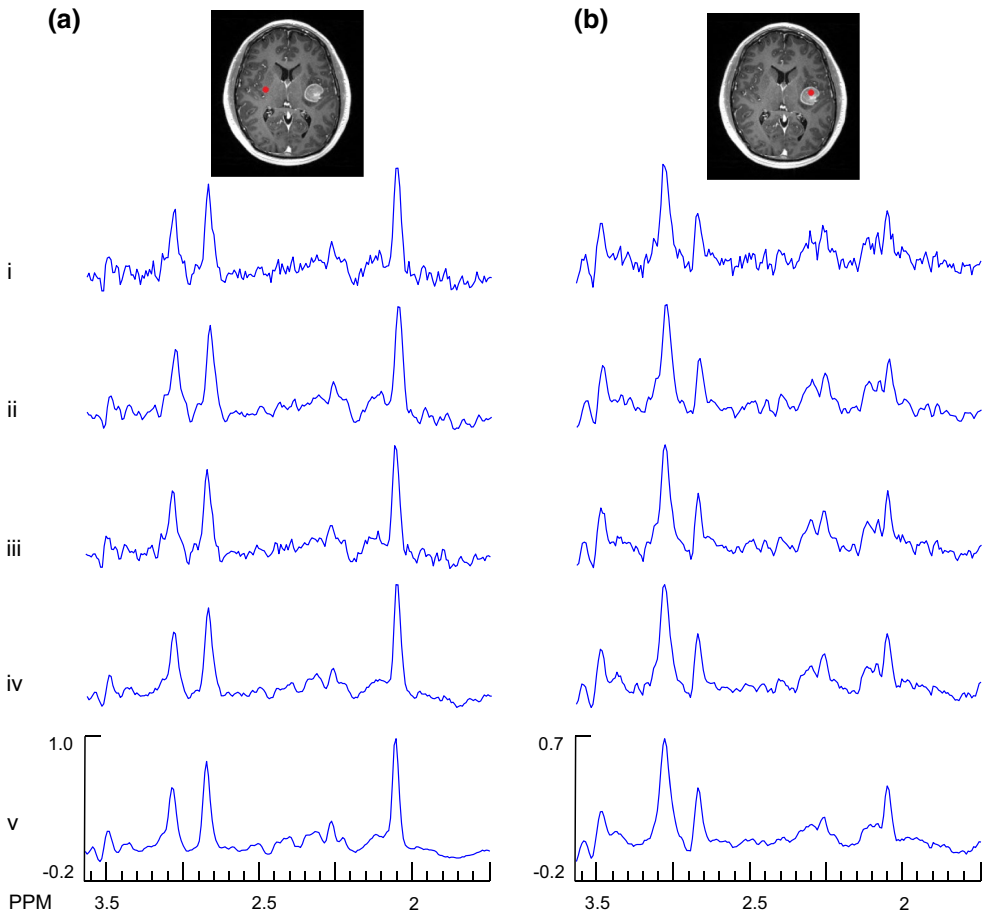


**Fig. 6** Example spectra from the denoising of an in vivo MRSI study of a subject with a brain tumor. Column **a** shows the results for a voxel selected from a normal-appearing white matter region (voxel 1), and column **b** shows the results for a voxel selected in the tumor region (voxel 2). The rows show results for the original data *(i)*, Gaussian denoising *(ii)*, PCA denoising using the first 119 PCs *(iii)*, SSPC denoising with a threshold of 1E−5 (the algorithm found 119 PCs for this threshold) *(iv)* and SSPC denoising with a threshold of 1E−10 (the algorithm found 56 PCs for this threshold) *(v)*

better for larger numbers of voxels that have the same spectral pattern. Similar results were demonstrated using the simulated MRS data presented in Table 1. The SSPC denoising with a threshold of 1E−10 resulted in the best CRB values with the exception of $CRB_{Glx}$ for voxel 2, which was due to the reduced Glx peak height (Fig. 6b (v)) in this region.

**Table 3** $CRB_{Cr}$, $CRB_{Glx}$ and SNR for the second in vivo experiment with the brain tumor

| | Voxel 1 | | | Voxel 2 | | |
|---|---|---|---|---|---|---|
| | $CRB_{Cr}$ | $CRB_{Glx}$ | SNR | $CRB_{Cr}$ | $CRB_{Glx}$ | SNR* |
| No denoising | 5.439 | 4.582 | 91.786 | 9.499 | 12.167 | 31.669 |
| Gaussian apodization | 4.403 | 3.640 | 106.486 | 8.306 | 11.302 | 41.833 |
| PCA (119) | 4.296 | 3.592 | 101.235 | 8.208 | 9.689 | 38.059 |
| SSPC (1E−5) | 3.617 | 3.413 | 186.706 | 7.078 | 10.600 | 52.614 |
| SSPC (1E−10) | 3.170 | 3.034 | 418.276 | 5.850 | 15.499 | 86.218 |

* For voxel 2, the SNR was calculated using the Cho area instead of NAA

Mean and standard deviation (SD) of the SNR were calculated for two ROIs, one located outside of the tumor region (25 voxels) and one within the tumor region (25 voxels). These results are presented in Table 4 and show that the SSPC denoising with a 1E−10 $p$ value threshold increased the SNR by factors of 2.3, 2.3 and 1.1 compared to Gaussian apodization (5 Hz), conventional PCA (with 119 PCs) and SSPC denoising (10E−5 threshold), respectively. For ROI 2, the SNR was calculated from the Cho area, since NAA was absent, and the SSPC denoising with 1E−10 $p$ value threshold resulted in a SNR increase of 2.3 times compared to the Gaussian apodization case.

**Table 4** Mean and SD of the SNR for two ROIs inside and outside of the tumor region

| | ROI 1 | | ROI 2 | |
|---|---|---|---|---|
| | Mean | SD | Mean | SD |
| No denoising | 108.7 | 20.8 | 40.9 | 10.8 |
| Gaussian apodization | 139.2 | 34.3 | 56.5 | 14.9 |
| PCA (119) | 138.7 | 36.8 | 59.2 | 16.2 |
| SSPC (1E−5) | 273.4 | 49.9 | 85.9 | 18.8 |
| SSPC (1E−10) | 315.0 | 50.2 | 131.4 | 22.2 |

For ROI 2, the SNR was calculated using the Cho area instead of NAA

## Discussion

This study has presented a PCA-based denoising method for MRSI data that incorporates PC selection based on a statistical comparison of spectral regions containing metabolite information and noise. The aim of this statistical examination was to examine the homogeneity of variances between the signal and noise regions derived from each PC. A threshold was then applied to the $p$ value of Levene's test to select PCs that contained significant metabolite information.

A primary finding of this study is that the SSPC denoising can significantly improve the SNR and metabolite quantification accuracy in simulated spectra, and reduce uncertainty in in vivo data, without significantly compromising the metabolite information, provided that a sufficient number of PCs are retained. This method also performed better compared to the conventional PCA-based method. Using both simulated and in vivo MRSI data, it was shown that the SSPC denoising resulted in a higher SNR and lower CRBs values compared to the conventional PCA denoising with the same number of PCs and that the relative performance varied spatially in a manner that depended on the number of spectra with similar spectral patterns. The SSPC denoising with a $p$ value threshold of 1E−10 showed the most improvements for the SNR and CRB values without altering the linewidth, although with some indication of a loss of information for small metabolite resonances [e.g., Fig. 6b (v)]. A $p$ value threshold of 1E−5 appears to offer a more conservative approach. The impact of PCA-based denoising on the uncertainty of spectral fitting as indicated by CRB values is also greater for lower concentration metabolites (e.g., $Glx_{Area}$) than for those with prominent resonances (e.g., $Cr_{Area}$), likely reflecting the improved performance of the spectral fitting algorithm used for this study with increasing SNRs.

Results of the third in vivo study with a small brain lesion also indicated good performance of the SSPC denoising in terms of SNR and fitting uncertainty; however, for a voxel located in the lesion the PCA denoising methods resulted in increased $CRB_{Glx}$ values with a threshold $p$ value of 1E−10. The reason for this decrease in performance is the small number of voxels with the spectral pattern characteristic of the lesion relative to the rest of the brain. This regional size dependency can be considered as one of the limitations of the PCA (or SVD) based denoising methods.

Limitations of this study include that the effects of residual baseline signals from unsuppressed water or lipid were not considered and that the effect of altered noise distributions on the spectral fitting algorithm was not specifically examined. If strong baseline signals are consistent and widespread they would be identified as signal-related and maintained in the result. However, commonly these signals are highly variable, and although those signal-related PCs will be identified, the corresponding eigenvalues for most

voxels will be small, and there will be minimal impact on the denoising performance.

## Conclusion

In summary, it was shown that the SSPC denoising improved the SNR and quantification accuracy using three simulated MRSI data sets and reduced quantification uncertainty in two in vivo data sets. In addition to providing good performance, this method is simple to implement and computationally efficient with the total computing time less than ~60 s for spectra from a volumetric in vivo data set.

**Acknowledgments** This work was supported by the National Institutes of Health grants R01EB016064 and R01CA172210. The authors thank Dr. M. Goryawala for assistance with data collection. Drs. Stoyanova and Maudsley are co-senior authors.

**Compliance with ethical standards**

**Conflict of interest** The authors declare that they have no conflict of interest.

**Ethical approval section** All procedures performed in studies involving human participants were in accordance with the ethical standards of the institutional and/or national research committee and with the 1964 Helsinki Declaration and its later amendments or comparable ethical standards.

**Informed consent section** Informed consent was obtained from all individual participants included in the study.

## References

1. Maudsley AA, Domenig C, Govind V, Darkazanli A, Studholme C, Arheart K, Bloomer C (2009) Mapping of brain metabolite distributions by volumetric proton MR spectroscopic imaging (MRSI). Magn Reson Med 61:548–559
2. Buades A, Coll B, Morel JM (2005) A review of image denoising algorithms, with a new one. Multiscale Model Simul 4:490–530
3. Bartha R, Drost DJ, Williamson PC (1999) Factors affecting the quantification of short echo in vivo 1H MR spectra: prior knowledge, peak elimination, and filtering. NMR Biomed 12:205–216
4. Cancino-De-Greiff HF, Ramos-Garcia R, Lorenzo-Ginori JV (2002) Signal de-noising in magnetic resonance spectroscopy using wavelet transforms. Concepts Magn Reson 14:388–401
5. Donoho DL, Johnstone Jain M (1994) Ideal spatial adaptation by wavelet shrinkage. Biometrika 81:425–455
6. Ojanen J, Miettinen T, Heikkonen J, Rissanen J (2004) Robust denoising of electrophoresis and mass spectrometry signals with minimum description length principle. FEBS Lett 570:107–113
7. Laruelo A, Chaari L, Batatia H, Ken S, Rowland B, Laprie A, Tourneret JY (2013) Hybrid sparse regularization for magnetic resonance spectroscopy. IEEE Eng Med Biol Soc, Osaka, pp 6768–6771
8. Ahmed OA (2005) New denoising scheme for magnetic resonance spectroscopy signals. IEEE Trans Med Imag 24:809–816
9. Ahmed OA, Fahmy MM (2001) NMR signal enhancement via a new time-frequency transform. IEEE Trans Med Imag 20:1018–1025
10. Eslami R, Jacob M (2009) Reduction of distortions in MRSI using a new signal model. IEEE Int Symp Biomed Imag, Boston, pp 438–441
11. Nguyen HM, Haldar JP, Do MN, Zhi-Pei L (2010) Denoising of MR spectroscopic imaging data with spatial-spectral regularization. IEEE Int Symp Biomed Imag, Rotterdam, pp 720–723
12. Lam F, Babacan SD, Haldar JP, Weiner MW, Schuff N, Liang ZP (2014) Denoising diffusion-weighted magnitude MR images using rank and edge constraints. Magn Reson Med 71:1272–1284
13. Lin X, Changqing W, Wufan C, Xiaoyun L (2014) Denoising multi-channel images in parallel MRI by low rank matrix decomposition. IEEE Trans Appl Supercond 24:1–5
14. Zhou X, Yang C, Zhao H, Yu W (2014) Low-rank modeling and its applications in medical image analysis. ACM Comput Surv 47:1–35
15. Stoyanova R, Brown TR (2001) NMR spectral quantitation by principal component analysis. NMR Biomed 14:271–277
16. Stoyanova R, Querec TD, Brown TR, Patriotis C (2004) Normalization of single-channel DNA array data by principal component analysis. Bioinformatics 20:1772–1784
17. Brown TR, Stoyanova R (1996) NMR spectral quantitation by principal-component analysis. II. Determination of frequency and phase shifts. J Magn Reson B 112:32–43
18. Stoyanova R, Brown TR (2002) NMR spectral quantitation by principal component analysis. III. A generalized procedure for determination of lineshape variations. J Magn Reson 154:163–175
19. Zhu XP, Du AT, Jahng GH, Soher BJ, Maudsley AA, Weiner MW, Schuff N (2003) Magnetic resonance spectroscopic imaging reconstruction with deformable shape-intensity models. Magn Reson Med 50:474–482
20. Nguyen HM, Peng X, Do MN, Liang ZP (2013) Denoising MR spectroscopic imaging data with low-rank approximations. IEEE Trans Biomed Eng 60:78–89
21. Kasten J, Lazeyras F, Van De Ville D (2013) Data-driven MRSI spectral localization via low-rank component analysis. IEEE Trans Med Imag 32:1853–1863
22. Shibata R (1976) Selection of the order of an autoregressive model by Akaike's information criterion. Biometrika 63:117–126
23. Gastwirth JL, Gel YR, Miao W (2009) The impact of Levene's test of equality of variances on statistical theory and practice. Stat Sci 24:343–360
24. Maudsley AA, Darkazanli A, Alger JR et al (2006) Comprehensive processing, display and analysis for in vivo MR spectroscopic imaging. NMR Biomed 19:492–503
25. Maudsley AA, Domenig C, Ramsay RE, Bowen BC (2010) Application of volumetric MR spectroscopic imaging for localization of neocortical epilepsy. Epilepsy Res 88:127–138
26. Sabati M, Sheriff S, Gu M, Wei J, Zhu H, Barker PB, Spielman DM, Alger JR, Maudsley AA (2015) Multivendor implementation and comparison of volumetric whole-brain echo-planar MR spectroscopic imaging. Magn Reson Med 74:1209–1220
27. Maudsley AA, Darkazanli A, Alger JR, Hall LO, Schuff N, Studholme C, Yu Y, Ebel A, Frew A, Goldgof D, Gu Y, Pagare R, Rousseau F, Sivasankaran K, Soher BJ, Weber P, Young K, Zhu X (2006) Comprehensive processing, display and analysis for in vivo MR spectroscopic imaging. NMR Biomed 19:492–503
28. Metzger G, Hu X (1997) Application of interlaced Fourier transform to echo-planar spectroscopic imaging. J Magn Reson 125:166–170

29. Abdoli A, Maudsley AA (2015) Phased-array combination for MR spectroscopic imaging using a water reference. Magn Reson in Med. doi:10.1002/mrm.25992
30. Haupt CI, Schuff N, Weiner MW, Maudsley AA (1996) Removal of lipid artifacts in 1H spectroscopic imaging by data extrapolation. Magn Reson Med 35:678–687
31. Soher BJ, Young K, Govindaraju V, Maudsley AA (1998) Automated spectral analysis III: application to in vivo proton MR spectroscopy and spectroscopic imaging. Magn Reson Med 40:822–831
32. Cadzow JA (1988) Signal enhancement-a composite property mapping algorithm. IEEE Trans Acoust Speech Signal Process 36:49–62